M&C 2017 - International Conference on Mathematics & Computational Methods Applied to Nuclear Science & Engineering, Jeju, Korea, April 16-20, 2017, on USB (2017)

2-D/3-D Reactor Analysis using Orthogonal-Mesh S_N with Embedded 2-D Method of Characteristics[1]

Mitchell T.H. Young*†, Benjamin Collins†, William R. Martin*

*University of Michigan, Ann Arbor, MI
†Oak Ridge National Laboratory, P.O. Box 2008, Oak Ridge, TN
youngmit@umich.edu

Abstract - *The Method of Characteristics (MOC) is a well-known and common approach for performing pin-resolved reactor neutronics simulations in 2-D, but has remained computationally impractical to extend directly to 3-D. 2-D/1-D methods have commonly been used instead to provide less expensive 3-D solutions, using a collection of 2-D MOC solvers to treat axial slices of the reactor and coupling them with a collection of 1-D solvers along each pin cell. These methods tend to work well under certain circumstances, but suffer poor accuracy and stability in others. In this work, a new 2-D/3-D approach was developed, which couples the 2-D MOC planes using a global 3-D S_N solver that operates on an orthogonal, pin-homogenized mesh. The S_N solver employs a pair of correction factors that are calculated using the MOC solvers to maintain accuracy on the coarse mesh. The 2-D/3-D method was applied to the C5G7 and Takeda benchmark problems. For the C5G7 benchmarks, 2-D/3-D produced results that were similar to or better than existing 2-D/1-D methods. For the Takeda cases, the 2-D/3-D method produced much better results and was able to converge a case that the 2-D/1-D methods failed to converge.*

I. INTRODUCTION

The Method of Characteristics (MOC) has seen much interest in the reactor analysis community, especially for its ability to obtain direct, pin-resolved solutions to the Boltzman transport equation. While MOC extends easily to 3-D from a theoretical standpoint, the computational expense of doing so is considerable and not currently feasible for full-core reactor simulations. Instead, a class of planar synthesis methods have been developed, generally referred to as 2-D/1-D methods. These methods take advantage of the prismatic nature of a reactor core by decomposing the reactor into a number of axial slabs, each treated with 2-D, pin-resolved MOC. A series of 1-D, pin-homogenized axial solvers are then used to treat the axial dimension. This approach has been adopted by numerous reactor analysis codes, such as CRX[1], DeCART[2], MPACT[3], and nTRACER[4].

2-D/1-D constitutes a class of methods, depending on the type of axial solver and transverse leakage approximations used. Most axial solvers employ some form of diffusion or P_N axial treatments. Many of these methods, especially those based on diffusion, suffer poor accuracy and convergence behavior in situations involving strong axial discontinuities or thin axial planes[5]. Furthermore, diffusion and P_N axial solvers become ill-conditioned in problems with void or near-void regions.

To address these issues, a new 2-D/3-D method was developed, which employs a global 3-D, pin-homogenized S_N sweeper in lieu of the 1-D axial solvers. A corrected diamond difference (CDD) S_N formulation is used to maintain accuracy and conditional equivalence between the S_N sweeper and its underlying 2-D MOC sweepers. In this work, we describe a number of such methods and apply them to the C5G7 benchmark rodded configurations and the Takeda Model 1 benchmark problems.

II. THEORY

The 2-D/3-D approach is based upon the discrete ordinates, multi-group form of the transport equation solved on an orthogonal grid. Having applied the discrete ordinates and multi-group discretizations in angle and energy, the transport equation has the form

$$\hat{\mathbf{\Omega}}^n \cdot \nabla \psi_g^n(\mathbf{r}) + \Sigma_{\mathrm{t},g}(\mathbf{r})\psi_g^n(\mathbf{r}) = \sum_{g' \in G} \sum_{n' \in N} w_n \Sigma_{\mathrm{s},g'g}^{n'n}(\mathbf{r})\psi_g^n(\mathbf{r}) + \frac{1}{k}\frac{\chi_g(\mathbf{r})}{4\pi} \sum_{g' \in G} \nu\Sigma_{\mathrm{f},g'}(\mathbf{r}) \sum_{n \in N} \psi_{g'}^n(\mathbf{r}) w_n. \quad (1)$$

Here, n is used to denote the discrete angle index and g is the energy group index. Going forward, the group index will be elided for brevity, and the scattering and fission sources are combined into a total source Q_{ijk}. Integrating Eq. (1) over an element of an orthogonal mesh bounded by $x_{i-1/2} < x < x_{i+1/2}$,

[1]This manuscript has been authored by UT-Battelle, LLC under Contract No. DE-AC05-00OR22725 with the U.S. Department of Energy. The United States Government retains and the publisher, by accepting the article for publication, acknowledges that the United States Government retains a non-exclusive, paid-up, irrevocable, world-wide license to publish or reproduce the published form of this manuscript, or allow others to do so, for United States Government purposes. The Department of Energy will provide public access to these results of federally sponsored research in accordance with the DOE Public Access Plan (http://energy.gov/downloads/doe-public-access-plan).

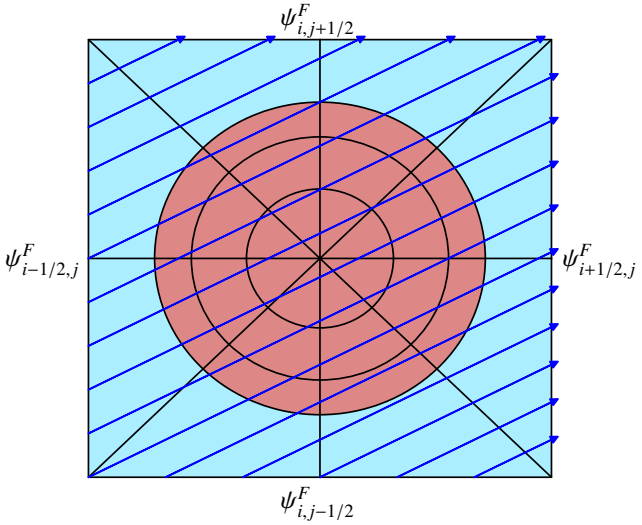

Fig. 1: MOC ray trace through a pin-homogenized mesh.

$y_{j-1/2} < y < y_{j+1/2}$, and $z_{k-1/2} < z < z_{k+1/2}$ gives

$$\frac{\eta^n}{\Delta x}\left(\psi^n_{i+1/2,j,k} - \psi^n_{i-1/2,j,k}\right) + \frac{\varepsilon^n}{\Delta y}\left(\psi^n_{i,j+1/2,k} - \psi^n_{i,j-1/2,k}\right) + \frac{\mu^n}{\Delta z}\left(\psi^n_{i,j,k+1/2} - \psi^n_{i,j,k-1/2}\right) + \Sigma_{\mathrm{t},ijk}\bar{\psi}^n_{ijk} = Q^n_{ijk}. \tag{2}$$

Assuming that the angular flux incident upon the mesh element are known, Eq. (2) constitutes a single equation with 4 unknowns. Previous work[6, 7] developed the CDD equations to provide closure to the above equation. These are similar in form to the classical diamond difference (DD) equations, but incorporate a pair of correction factors, which enforce streaming and collision behavior from an underlying fine-mesh solution:

$$\bar{\psi}^n = \beta^n_{ijk}\alpha^n_{x,ijk}\left(\psi^n_{i+1/2,j,k} + \psi^n_{i-1/2,j,k}\right) \text{ and} \tag{3a}$$

$$\bar{\psi}^n = \beta^n_{ijk}\alpha^n_{y,ijk}\left(\psi^n_{i,j+1/2,k} + \psi^n_{i,j-1/2,k}\right). \tag{3b}$$

The terms $\alpha^n_{x,ijk}$ and $\alpha^n_{y,ijk}$ are *streaming correction factors*, calculated using known streaming behavior from a fine-mesh MOC sweep as

$$\alpha^n_{x,ijk} = \frac{\bar{\psi}^{n,F}_{ijk}}{\psi^{n,F}_{i+1/2,j,k} + \psi^{n,F}_{i-1/2,j,k}} \text{ and} \tag{4a}$$

$$\alpha^n_{y,ijk} = \frac{\bar{\psi}^{n,F}_{ijk}}{\psi^{n,F}_{i,j+1/2,k} + \psi^{n,F}_{i,j-1/2,k}}, \tag{4b}$$

where $\bar{\psi}^F_{ij}$ is the MOC angular flux homogenized onto coarse mesh element (i, j, k). The terms $\psi^F_{i\pm1/2,j,k}$ and $\psi^F_{i,j\pm1/2,k}$ are the MOC angular flux averaged over the x- and y-normal coarse mesh surfaces, respectively, as depicted in Fig. 1.

A *collision correction factor*,

$$\beta^n_{ijk} = \frac{\bar{\Sigma}^n_t}{\Sigma_t}, \tag{5}$$

preserves the reaction rates from the fine-mesh MOC sweeper within the coarse-mesh S_N mesh element. In the definition of β_{ijk}, $\bar{\Sigma}^n_t$ is an angular flux-weighted total cross section, also determined using the fine-mesh MOC sweeper. These correction factors ($\beta^n\alpha^n_{x,ijk}$ and $\beta^n\alpha^n_{y,ijk}$) must be stored for each angle, energy group and pin cell. While this does carry a memory burden, as we discuss later this burden is minor under most realistic circumstances.

For 2-D problems it can be shown that using converged correction factors in a coarse-mesh S_N sweeper will yield an equivalent solution to the fine-mesh 2-D MOC sweeper that produced them. Since the correction factors are being determined using a 2-D sweeper, extension to 3-D problems requires an un-corrected auxiliary relation to treat the axial dimension in the S_N solver. In this work we consider the conventional diamond difference and step characteristics schemes.

1. Diamond difference axial treatment

The uncorrected diamond difference equation,

$$\bar{\psi}^n = \frac{1}{2}\left(\psi^n_{i,j,k+1/2} + \psi^n_{i,j,k-1/2}\right), \tag{6}$$

along with the Eqs. (3) can be used to eliminate the cell-exiting fluxes from Eq. (2) producing an expression for the cell-average flux,

$$\bar{\psi}_{ijk} = \frac{Q_{ijk} + 2\left(\frac{\eta}{\Delta x_i}\psi_{i\mp1/2,j,k} + \frac{\varepsilon}{\Delta y_j}\psi_{i,j\mp1/2,k} + \frac{\mu}{\Delta z_k}\psi_{i,j,k\mp1/2}\right)}{\frac{\eta}{\Delta x_i\beta\alpha_{x,ijk}} + \frac{\varepsilon}{\Delta y_j\beta\alpha_{y,ijk}} + \frac{2\mu}{\Delta z_k} + \Sigma_{t,ijk}}, \quad \eta \gtrless 0, \quad \varepsilon \gtrless 0, \quad \mu \gtrless 0. \tag{7}$$

Cell-exiting fluxes are then calculated using Eqs. (3) and (6).

The diamond difference scheme is very rudimentary and computationally inexpensive, but it is not unconditionally positive; under certain conditions it can lead to negative angular fluxes. While occasional negative fluxes may be tolerated, they tend to lead to convergence issues, and may even result in negative scalar fluxes. To avoid this, it sometimes becomes necessary to apply a negative flux fix-up, where negative cell-exiting fluxes are set artificially to zero and the cell-average flux is recalculated using a modified difference relation. While running the benchmarks discussed in this work, the negative flux fix-up approach was necessary to converge some of the cases discussed below.

2. Step characteristics axial treatment

The well-known step characteristics scheme[8] was also used to treat the axial dimension. This scheme can be written as

$$\bar{\psi}^n_k = \rho^n_k\psi^n_{k\mp1/2} + \left(1 - \rho^n_k\right)\psi^n_{k\pm1/2}, \quad \mu^n \gtrless 0, \tag{8}$$

where

$$\rho^n_k = \frac{1}{\tau^n_k} - \frac{1}{e^{\tau^n_k} - 1} \tag{9}$$

and τ^n_k is the apparent optical thickness of cell k for angle n,

$$\tau^n_k = \frac{\Sigma_{t,k}\Delta z_k}{|\mu^n|}. \tag{10}$$

Using this along with the CDD equations in Eq. (2) produces the following expression for the cell-average flux:

$$\bar{\psi}_{ijk} = \frac{Q_{ijk} + \frac{2\eta}{\Delta x_i}\psi_{i\mp 1/2,j,k} + \frac{2\varepsilon}{\Delta y_j}\psi_{i,j\mp 1/2,k} + \frac{\mu}{\Delta z_k(1-\rho)}\psi_{i,j,k\mp 1/2}}{\frac{\eta}{\Delta x_i \beta\alpha_{x,ijk}} + \frac{\varepsilon}{\Delta y_j \beta\alpha_{y,ijk}} + \frac{\mu}{\Delta z_k(1-\rho)} + \Sigma_{tr,ijk}},$$
$$\eta \gtrless 0, \quad \varepsilon \gtrless 0, \quad \mu \gtrless 0. \tag{11}$$

The step characteristic scheme tends to be less accurate than the diamond difference scheme, but has the beneficial feature that given positive cross sections and sources, it will always produce positive fluxes.

3. S_N-MOC coupling

In previous work[6, 7], a one-way coupling method was employed, in which separate eigenvalue solutions were obtained for each axial slab of a reactor using a 2-D MOC solver. At convergence, correction factors and flux-weighted cross sections were calculated on a pin-homogenized mesh using the resulting flux distribution. These were then composed to form a 3-D mesh representing the global problem, and a CDD-based S_N was used to obtain the global solution. This method had a number of drawbacks. First, axial streaming effects were neglected in the calculation of the S_N data, affecting the accuracy of the MOC solutions used to determine the correction factors and cross sections. Second, it presented difficulty in treating axial regions with little or no fissile material, because the resulting 2-D eigenvalue problem would either be impossible, or wildly unrepresentative of the actual system being simulated. In such cases, it became necessary to use less-accurate volume-weighted cross sections and eschew correction factors entirely in those regions.

In this work, a two-way coupling scheme –very similar to existing 2-D/1-D methods– is employed, in which transverse leakage sources determined using the 3-D S_N sweeper are used to inform the 2-D MOC plane sweepers of axial streaming behavior. Transverse leakage arises from performing an axial decomposition of the reactor into slabs and integrating Eq. (1) over the height of each slab, giving

$$\left(\eta^n \frac{\partial}{\partial x} + \varepsilon^n \frac{\partial}{\partial y}\right)\psi_g^n(x,y) + \Sigma_{t,g}\psi_g^n(x,y) + L(x,y)_n^g = Q_g^n(x,y), \tag{12}$$

where $L(x,y)_g^n$ is the transverse leakage term,

$$\begin{aligned} L(x,y)_g^n &= \frac{\mu^n}{h_z}\left(\psi_{g,T}^n(x,y) - \psi_{g,B}^n(x,y)\right) \\ &\approx \frac{\mu^n}{h_z}\left(\psi_{g,T}^n - \psi_{g,B}^n\right) \\ &\approx \frac{J_g^T - J_g^B}{h_z}. \end{aligned} \tag{13}$$

Here we have made the flat-in-space, isotropic-in-angle approximation that is common among 2-D/1-D methods. In practice, the transverse leakage is usually applied by subtracting it to the left-hand side of Eq. (12) and incorporating it into the source variable.

Using the above transverse leakage definition, the S_N and MOC sweepers are coupled within a power iteration to converge the system eigenvalue and flux distribution. For each power iteration, the following steps are performed:

1. An updated global, coarse-mesh flux distribution and system eigenvalue are obtained using the CMFD acceleration technique[9].
2. Axial currents from the CMFD solution are used to compute transverse leakage sources, which are applied to the planar MOC sweepers.
3. A number of MOC sweeps are performed on each plane. Following the last MOC sweep, CDD correction factors and flux-weighted cross sections are calculated on the S_N mesh.
4. A number of S_N sweeps are performed using the correction factors and cross sections calculated by the MOC sweepers. During the last S_N sweep, cell interface currents are calculated to be used by the CMFD accelerator.

This process is repeated until converged.

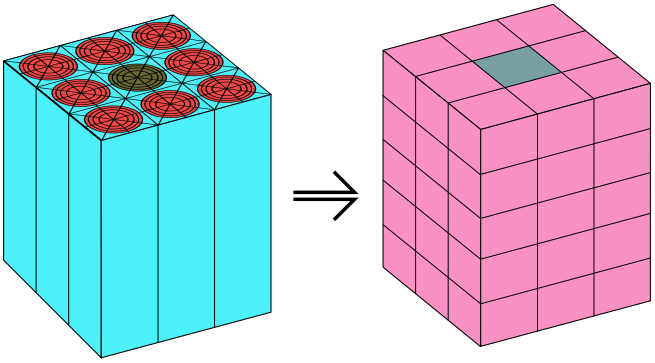

Fig. 2: Meshes used for the MOC (left) and S_N (right) sweepers.

The MOC sweeper operates on a pin-resolved mesh in the x and y directions, but is usually rather coarse in the axial dimension. The S_N sweeper operates on pin-homogenized mesh, but with potentially smaller axial regions, as depicted in Fig. 2. This allows for the S_N sweeper to better resolve axial behavior without requiring an accordingly large number of MOC planes.

III. RESULTS AND ANALYSIS

The 2-D/3-D methods described above were applied to the 3-D C5G7[10] and Takeda[11] benchmark problems, along with the old one-way 2-D/3-D method. 2-D/1-D methods based on the Nodal Expansion Method (NEM) and P_3 axial solvers were also used for comparison. The C5G7 cases were used to demonstrate accuracy and computational performance of the methods in a Light Water Reactor (LWR)-like scenario. The Takeda cases feature a smaller critical system with strong 3-D material discontinuities and a near-void region, both of which stress common 2-D/1-D methods.

The 2-D/3-D results were obtained using MOCC[12], a new MOC code developed as a test bed for such methods, while the 2-D/1-D results were obtained using the MPACT code. All methods used identical mesh, ray, and angular discretizations for each problem. The various methods are referred to using the following abbreviations:

- **2D1D NEM**: 2-D/1-D with NEM axial treatment.

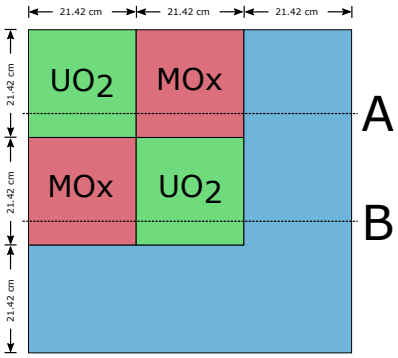

Fig. 3: C5G7 top view.

- **2D1D P3**: 2-D/1-D with P_3 axial treatment.
- **2W CDD-DDFF**: 2-D/3-D with two-way coupling, diamond difference axial treatment and negative flux fix-up.
- **2W CDD-DD**: 2-D/3-D with two-way coupling, CDD correction factors, diamond difference axial treatment, no negative flux fix-up.
- **2W CDD-SC**: 2-D/3-D with two-way coupling, CDD correction factors, step characteristics axial treatment.
- **1W DD**: 3-D S_N using diamond difference with flux-weighted cross sections from standalone 2-D MOC solutions.
- **1W CDD-DD**: 3-D S_N with CDD correction factors and flux-weighted cross sections. Uncorrected diamond difference axial treatment.

1. C5G7 Benchmarks

The C5G7 benchmark is a small, 4-by-4 assembly reactor typically modeled in 1/8 symmetry. The assemblies in the active core region are 17-by-17 arrays of fuel pins of various compositions and control rods/guide tubes. The benchmark is comprised of three cases with different control rod configurations, depicted in Figs. 3-6. The hashing in Figs. 4-6 indicate the presence of control rods at in each assembly and axial level.

Each configuration was simulated using all of the above methods. For the cylindrical pins, a mesh similar to the one depicted in Fig. 1 was used with 5 radial rings in the non-moderator regions, 2 extra rings in the moderator and 8 azimuthal subdivisions throughout. Homogeneous regions, such as in the radial reflector were represented using a rectangular mesh with 5 equally-spaced subdivisions in the x and y directions per unit cell. The rays were spaced at a nominal distance of 0.05 cm, using a Chebychev quadrature with 16 azimuthal angles and a Gauss quadrature with 4 polar angles per octant, for a total of 64 angles per octant. All MOC plane heights were 3.57 cm, yielding a total of 18 MOC planes. For the 2-D/3-D cases, the S_N sweeper operated on a 0.714 cm axial mesh, giving 5 S_N mesh regions per MOC plane.

A. Accuracy

Eigenvalue results are presented in Table I. The aggregate pin power metrics of average error (AVG), mean relative error

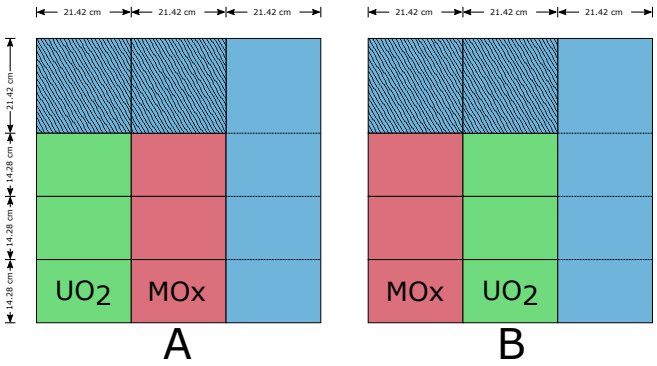

Fig. 4: C5G7 unrodded configuration side view.

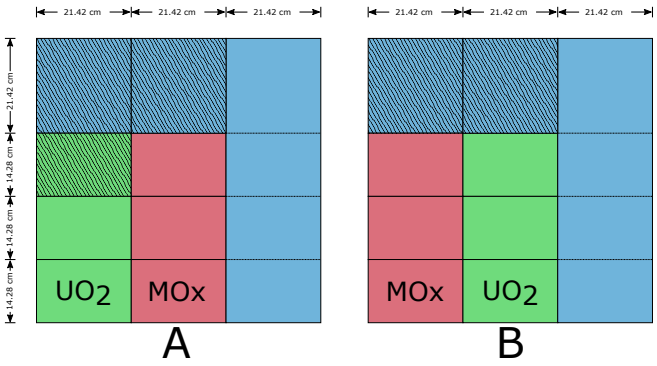

Fig. 5: C5G7 rodded configuration A side view.

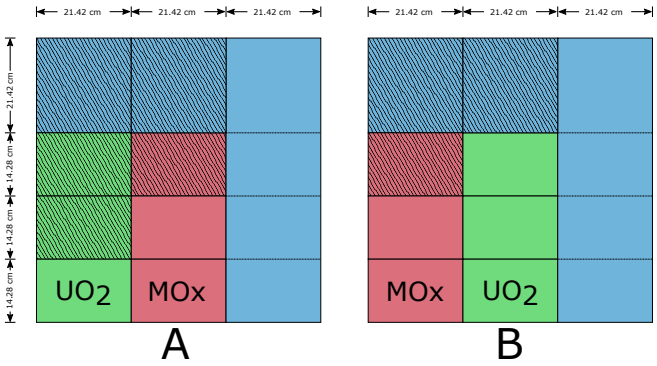

Fig. 6: C5G7 rodded configuration B side view.

(MRE) and root mean squared (RMS) error,

$$\text{AVG} = \frac{\sum_N |e_n|}{N}$$

$$\text{RMS} = \sqrt{\frac{\sum_N e_n^2}{N}}$$

$$\text{MRE} = \frac{\sum_N |e_n| \cdot p_n}{N \cdot p_{avg}},$$

are presented in Table II.

The two-way coupling methods show good performance at predicting system eigenvalue; they are uniformly better than 2-D/1-D NEM, but similar or somewhat worse in accuracy to the 2-D/1-D P_3. On the other hand, the pin power predictions of the CDD 2-D/3-D methods were better than both the NEM and P_3 methods, suggesting that the 2-D/3-D method produces a more accurate spatial flux distribution. Comparing results between the 2W CDD-DD and 2W CDD-DDFF methods demonstrates that the negative flux fix-up has little effect on the unrodded and rodded A cases, but considerable impact on the accuracy in the rodded B case. The rodded B case exhibits more drastic axial discontinuities and therefore produces more negative fluxes. It should be noted that the unrodded and rodded B cases would not converge with CMFD acceleration enabled without the negative flux fix-up. The step characteristic axial treatment tended to produce only slightly worse results than the diamond difference axial treatment.

B. Spatial variation of correction factors

Comparisons were also made between the CDD correction factors produced using the one-way and two-way schemes. Figure 7 shows the axial variation of the correction factors along a single fuel pin within a MOX assembly from rodded configuration B. To aid in visualization, an angular integral of the variation of the correction factors from their trivial value is presented, rather than the factors themselves. In some regions, the two-way factors vary appreciably from their one-way counterparts, especially in the vicinity of control rod tips. This highlights the importance of incorporating transverse leakage in the MOC calculations when calculating suitable correction factors.

C. Computational cost

Since many aspects of the 2-D/3-D and 2-D/1-D methods are nearly identical, an effective means by which to assess their relative runtime costs is to compare the fraction of time spent in the "axial" solver rather than the MOC solver. In all of these cases, the 2-D/1-D NEM axial solver constituted about 2% of the solve time, while the 2-D/1-D P_3 method used around 12%. By contrast, the two-way 2-D/3-D methods spent approximately 25% of the solve time in the S_N sweeper. This indicates that as implemented, the 2-D/3-D methods are more expensive than most 2-D/1-D methods.

Furthermore, storage of the correction factors requires extra memory. For the cases presented, a total of about 1.2 GB was needed to store these factors. In a more realistic full-core case, this would closer to the range of 80-90 GB, though it should be noted that such analyses are typically performed using thousands of CPU cores, leading to a memory burden of mere tens of MB per core.

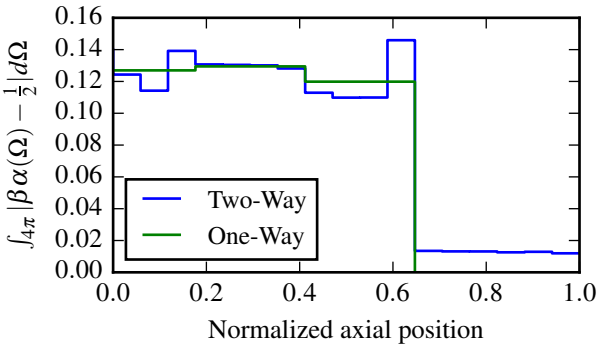

Fig. 7: Axial variation of CDD correction factors with and without transverse leakage coupling for a fuel pin in a MOX assembly from rodded configuration B, group 1.

2. Takeda Benchmark

The C5G7 benchmarks tend to be well suited for the 2-D/1-D methods, which behaved well and produced good results. However, Model 1 from the Takeda benchmarks (depicted with 1/8 symmetry in Fig. 8) presents more of a challenge to 2-D/1-D methods due to the presence of a void region and stronger axial streaming effects. Model 1 is a two-group problem consisting of a 15 cm cube of fissile material in a 10 cm blanket of polyethylene moderator. Two control rods can be inserted through channels on either side of the core region. In Case 2, these control rods are inserted. In Case 1, the rods are removed, leaving behind a voided region. The void region in Case 1 presents a challenge to most 2-D/1-D methods, since the underlying diffusion- and P_N-based axial solvers become ill-conditioned when the total cross section becomes small. This makes the Takeda benchmark a good candidate for 2-D/3-D methods, which are less susceptible to these issues.

Both cases were simulated using the 2-D/3-D CDD-DDFF method and the 2-D/1-D NEM and P_3 methods. Again, all methods employed the same discretization; the MOC sweepers used a relatively fine square mesh where $\Delta x = \Delta y = \frac{1}{15}$cm and a plane height of 5 cm. The S_N sweeper operated on a 1 cm cube mesh, for 5 axial S_N regions per MOC plane. The 2-D/1-D methods were unable to converge the first case with the void regions, but did manage to produce results for the rodded case. Eigenvalue results are presented in Table III, along with their variation from the published reference solution. Table IV contains the errors in the calculated region-averaged fluxes compared to the published reference solution.

Figure 9 presents the streaming correction factors for energy group 1 and the angle indicated by the arrow at the system mid-plane. Spatial variation of the correction factors exhibit some interesting behavior. For the indicated angle, the y correction factors vary considerably more than the x factors from

TABLE I: Eigenvalues for all three C5G7 cases using various methods.

	Unrodded		Rodded A		Rodded B	
	Eigenvalue	Error	Eigenvalue	Error	Eigenvalue	Error
Reference	1.14308	±6.0	1.12806	±6.0	1.07777	±6.0
2D1D NEM	1.14220	-88.16	1.12727	-78.90	1.07635	-141.87
2D1D P3	1.14281	-27.49	1.12791	-15.25	1.07745	-31.68
2W CDD-DDFF	1.14328	20.29	1.12849	43.44	1.07714	-63.34
2W CDD-DD	1.14328	20.13	1.12849	43.46	1.07819	42.34
2W CDD-SC	1.14276	-31.51	1.12764	-41.72	1.07691	-85.97
1W DD	1.14435	126.75	1.12876	70.44	1.07560	-217.07
1W CDD-DD	1.14286	-21.67	1.12831	24.99	1.07814	37.46

TABLE II: C5G7 2-D pin power metrics.

	Unrodded			
	AVG	MRE	RMS	Max Error
2D1D NEM	0.57%	2.79%	0.61%	2.94%
2D1D P3	0.57%	2.78%	0.61%	2.97%
2W CDD-DDFF	0.38%	1.79%	0.44%	2.44%
2W CDD-DD	0.38%	1.79%	0.44%	2.44%
2W CDD-SC	0.40%	1.75%	0.45%	2.24%
1W DD	1.59%	9.56%	2.08%	6.85%
1W CDD-DD	0.38%	1.80%	0.44%	2.56%
	Rodded A			
	AVG	MRE	RMS	Max Error
2D1D NEM	0.57%	3.55%	0.62%	2.66%
2D1D P3	0.57%	3.63%	0.62%	2.68%
2W CDD-DDFF	0.38%	2.40%	0.45%	2.16%
2W CDD-DD	0.38%	2.40%	0.45%	2.16%
2W CDD-SC	0.41%	2.20%	0.48%	2.15%
1W DD	1.49%	10.77%	1.84%	7.64%
1W CDD-DD	0.38%	2.72%	0.45%	2.09%
	Rodded B			
	AVG	MRE	RMS	Max Error
2D1D NEM	0.61%	4.09%	0.72%	3.12%
2D1D P3	0.57%	4.17%	0.64%	2.76%
2W CDD-DDFF	0.43%	3.10%	0.51%	2.43%
2W CDD-DD	0.38%	2.79%	0.47%	2.29%
2W CDD-SC	0.46%	3.19%	0.56%	2.52%
1W DD	1.64%	13.88%	2.04%	9.52%
1W CDD-DD	0.38%	3.04%	0.47%	2.17%

their trivial value of $\frac{1}{2}$, especially near material discontinuities. This is expected because the presented angle has a very small y component, which has the effect of stretching the apparent optical thickness of each cell along the y direction. This lengthening of the cells would lead to a less accurate result in the S_N sweeper if uncorrected diamond difference were used. Therefore a larger correction is required to maintain conformance with the better-resolved MOC solution. In general, the correction factors in the interior of the homogeneous regions are very close to their trivial values.

Comparing the Case 2 results shows that the 2-D/3-D method greatly out-performed the 2-D/1-D methods in predicting the system eigenvalue and region fluxes. Furthermore, the NEM and P_3 methods required 28 and 20 iterations to converge, respectively, while the 2-D/3-D method required only 8 iterations.

The improved accuracy and convergence behavior of the 2-D/3-D results suggest that the method is especially valuable for certain types of systems which do not lend themselves well to existing 2-D/1-D methods.

TABLE III: Eigenvalue results and error for Takeda Model 1.

Case 1	
Reference	0.97800 ±0.0006
2-D/1-D NEM	-
2-D/1-D P_3	-
2-D/3-D CDD-DDFF	0.97728 (-73 pcm)
Case 2	
Reference	0.96240 ±0.0006
2-D/1-D NEM	0.95325 (-950 pcm)
2-D/1-D P_3	0.95812 (-445 pcm)
2-D/3-D CDD-DDFF	0.96245 (6 pcm)

IV. CONCLUSIONS

With the application of a transverse leakage-based two-way coupling scheme, the 2-D/3-D method continues to show promise. Accuracy is shown to be on par with existing and commonly-used 2-D/1-D methods under typical LWR conditions. Under different circumstances with strong axial stream-

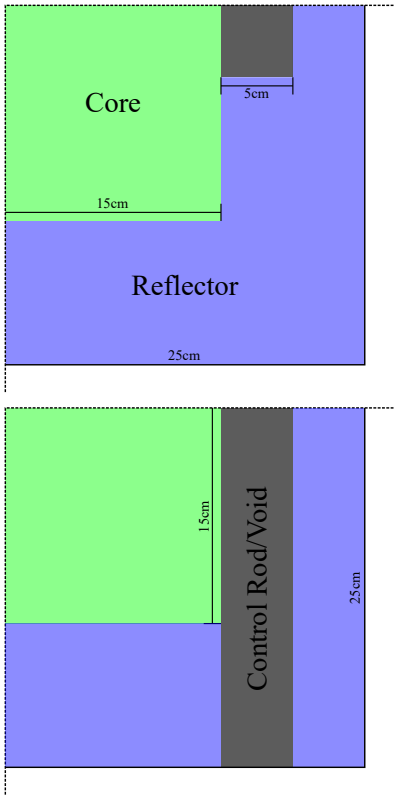

Fig. 8: Takeda benchmark Model 1 geometry.

TABLE IV: Variation of region-averaged scalar flux from published reference solution for Takeda Model 1.

	2-D/1-D NEM			
	Case 1		Case 2	
	Group 1	Group 2	Group 1	Group 2
Core	-	-	-1.547%	0.035%
Reflector	-	-	4.443%	4.435%
Control Rod	-	-	0.516%	1.069%
	2-D/1-D P_3			
	Case 1		Case 2	
	Group 1	Group 2	Group 1	Group 2
Core	-	-	-0.845%	-0.090%
Reflector	-	-	1.559%	1.872%
Control Rod	-	-	0.301%	0.076%
	2-D/3-D CDD-DDFF			
	Case 1		Case 2	
	Group 1	Group 2	Group 1	Group 2
Core	0.228%	0.215%	-0.376%	-0.173%
Reflector	0.360%	0.172%	-0.066%	0.232%
Control Rod	0.152%	-0.112%	0.073%	-0.082%

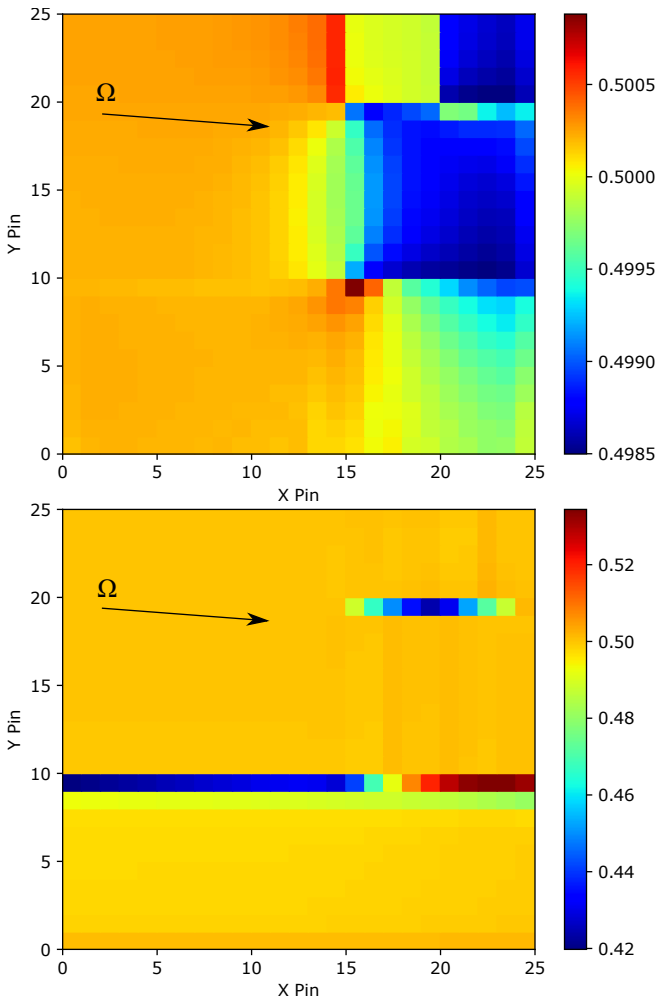

Fig. 9: Streaming correction factors α_x (top) and α_y (bottom) for group 1 and the angle indicated from the core midplane of Takeda Model 1, Case 2.

ing effects and void regions, such as the Takeda benchmark, the 2-D/3-D method greatly out-performs typical 2-D/1-D methods. Runtime and memory costs could still use improvement, however, and S_N optimizations and more efficient methods of storing the correction factors are important areas for future work. With the increasing importance of heterogeneous architectures and on-node parallelism, the S_N portion of a 2-D/3-D solver is a prime candidate for offloading to a GPU or similar co-processor. Work at ORNL[13] has shown that speedups of orthogonal-mesh S_N sweeps are indeed possible on the GPU.

So far, the 2-D/3-D method has only been applied to relatively simple benchmark problems with small systems and few energy groups. To gain confidence in the 2-D/3-D method for real full-core reactor analyses with much larger spatial domains and realistic cross sections, more complicated systems need to be simulated. Implementation of the 2-D/3-D method in a production-quality code such as MPACT will allow access to such applications, such as the CASL AMA benchmark problems[14] or the MIT BEAVRS benchmark[15].

V. ACKNOWLEDGMENTS

This research was supported by the Consortium for Advanced Simulation of Light Water Reactors (www.casl.gov), an Energy Innovation Hub (http://www.energy.gov/hubs) for Modeling and Simulation of Nuclear Reactors under U.S. Department of Energy Contract No. DE-AC05-00OR22725

REFERENCES

1. G. S. LEE and N. Z. CHO, "2D/1D fusion method solutions of the three-dimensional transport OECD benchmark problem C5G7 MOX," *Progress in Nuclear Energy*, **48**, 410–423 (2006).
2. H. G. JOO, J. Y. CHO, K. S. KIM, C. C. LEE, and S. Q. ZEE, "Methods and Performance of a Three-Dimensional Whole-Core Transport Code DeCART," *PHYSOR - The Physics of Fuel Cycles and Advanced Nuclear Systems, Lagrange Park, IL* (2004).
3. MPACT TEAM, "MPACT Theory Manual," Tech. rep., CASL-U-2015-0078-000, Oak Ridge National Laboratory and University of Michigan (2015).
4. Y. S. JUNG, C. B. SHIM, C. H. LIM, and H. G. JOO, "Practical numerical reactor employing direct whole core neutron transport and subchannel thermal/hydraulic solvers," *Annals of Nuclear Energy*, **62**, 357–374 (Nov. 2013).
5. B. W. KELLEY and E. W. LARSEN, "2D/1D Approximations to the 3D Neutron Transport Equation. I: Theory," *Proc. American Nuclear Society, Mathematics and Computation, Sun Valley, ID*, pp. 1346–1357 (2013).
6. M. T. H. YOUNG, B. COLLINS, and W. R. MARTIN, "2-D/3-D Coupling Between the Method of Characteristics and Discrete Ordinates," *Trans. of the American Nuclear Society*, **109**, 699–702 (2013).
7. M. T. H. YOUNG, B. S. COLLINS, and W. R. MARTIN, "Corrected diamond difference method for coupling from the method of characteristics to discrete ordinates," *PHYSOR: International Topical Meeting on Advances in Reactor Physics* (2014).
8. K. LATHROP, "Spatial Differencing of the Transport Equation: Positivity vs. Accuracy," *Journal of Computational Physics*, **4**, 475–498 (1969), step characteristics, Wendroff scheme.
9. K. S. SMITH, "Assembly Homogenization Techniques for Light Water Reactor Analysis," *Progress in Nuclear Energy*, **17**, *3*, 303–335 (1986).
10. M. SMITH and E. LEWIS, "Benchmark on Deterministic Transport Calculations Without Spatial Homogenisation: MOX Fuel Assembly 3-D Extension Case," Tech. Rep. NEA/NSC/DOC(2005)16, Nuclear Energy Agency Organisation for Economic Co-Operation and Development (2005).
11. T. TAKEDA and H. IKEDA, "3-D Neutron Transport Benchmarks," Tech. rep., Departement of Nuclear Engineering, Osaka University; OECD/NEA Committee on Reactor Physics (NEACRP).
12. M. T. H. YOUNG, "MOCC: A method of characteristics-based nuclear reactor physics simulator," https://github.com/youngmit/mocc (2016).
13. C. BAKER, G. DAVIDSON, T. M. EVANS, S. HAMILTON, J. JARRELL, and W. JOUBERT, "High Performance Radiation Transport Simulations: Preparing for TITAN," *SC 2012 Proceedings of the International Conference on High Performance Computing, Networking, Storage and Analysis* (2012).
14. A. T. GODFREY, "VERA Core Physics Benchmark Progression Problem Specifications," (2013), aMA advanced modeling and applications.
15. N. HORELIK, B. H. B. FORGET, and K. SMITH, "Benchmark for Evaluation and Validation of Reactor Simulations (BEAVRS)," *ANS MC2013* (2013).